Arabian Journal of Geosciences (2024) 17:235
https://doi.org/10.1007/s12517-024-12036-w

ORIGINAL PAPER

Reservoir recovery study with stability analysis model constructed by water-driven oil flat sand filling experiment: example of well area X in Tankou oilfield, China

Yuan Yang[1,2] **· Bo Liang**[3]

Received: 4 October 2023 / Accepted: 5 July 2024 / Published online: 20 July 2024

Abstract

The study of the law and degree of injection and extraction coupling in old oil areas is a difficult point that affects the recovery rate. The traditional experimental and numerical simulation research methods lack validation and working condition prediction. This study has improved the working steps and supplemented the lack of program validation link through the methods of data prediction and mathematical argumentation. This program has been implemented in the Tamkou field. In addition, we determined the relationship between different permeability, crude oil viscosity, and recovery rate influencing factors on recovery under the premise of a fixed well network, and the DGM (1,1) model prediction yielded the recovery rates of 8.93 and 12.08 for the next 2 time nodes. The analyses showed that adopting the means of water blending and dosing to adjust the crude oil viscosity to 90 mPa s, and adopting the water injection rate of 5 mL/min to extract the best recovery rate. Min water injection rate is optimal for extraction.

Keywords Flat sand fill experiment · DGM (1:1) · Oil recovery · Permeability · Oil viscosity

Introduction

The complex fault block reservoirs located in east-central China are predominantly siliciclastic sedimentary reservoirs with numerous oil layers and severe non-uniformity. To improve the recovery of residual oil without deploying new wells to densify the well network, most of the old oil fields have been studying the method of injection and extraction coupling (Liao et al. 2023; Wang et al. 2023a, b). Therefore, it is of great practical significance to clarify the issues of layer heterogeneity, within-layer heterogeneity, and plane heterogeneity, and to explore the flow fixation problems in the direction of the original fluid flow for the development and adjustment of old oil fields.

Currently, research on injection and recovery coupling for residual oil recovery focuses primarily on mechanism, physical experiments, and oilfield applications. Sun et al. (2023) conducted sand-filled tube experiments for CO_2 mixed-phase oil drive in tight reservoirs, proposed the correlation between tripropylene glycol (TPG) and CO_2 concentration, and further fitted a mathematical model for mixed-phase leading edge transport, and concluded that the most important parameter affecting CO_2 breakthrough is the injection rate. Chen et al. (2023) addressed the issue of how to reduce energy consumption in the development of high water-bearing oil fields, established a comprehensive energy consumption calculation model for the three stages of water injection-reservoir-extraction, and implemented the proposed scheme through a particle swarm optimization algorithm. Zhai et al. (2023), on the other hand, proposed a new multilateral horizontal well network accounting model for geothermal development in HDR (fractured heavy oil reservoir) reservoirs, and analyzed the sensitivity of the results through changes in well networks and injection and extraction parameters to assess the heat production potential. Liu et al. (2022) conducted a study on the

Responsible Editor: Santanu Banerjee

✉ Bo Liang
lglxr2021@163.com

[1] Exploration and Development Research Institute, Jianghan Oilfield Company, Sinopec 430223, Wuhan, China

[2] Key Laboratory of Oil and Gas Resources and Exploration Technology, Ministry of Education, School of Petroleum Engineering, Yangtze University, Wuhan 430100, China

[3] School of Aviation and Transportation, Jiangsu College of Engineering and Technology, Nantong 226000, China

deformation mechanism and deformation law of natural/artificial fractures and matrix pore space for the fracturing and injection process of unconventional tight reservoirs, focusing on exploring the relationship between fluid injection energy replenishment and development life cycle. A dynamic change model of multi-media geometry, physical properties, and inflow rate was proposed. Zheng and Sharma (2022) proposed a fully coupled reservoir-fracture-borehole model that implemented fluid flow, solid mechanics, energy balance, fracture extension, and particle filtration modelled in the reservoir, fracture, and borehole domains; while Kesarwani et al. (2022) conducted a study on surfactant polymers. Experimental analysis of α-MnO_2 nanoparticle additives was carried out for the oil drive process, resulting in a 70% increase in recovery. Aleidan et al. (2016) explored the remaining distribution characteristics by comparing information (filling time, hydrocarbon value content, chemical characteristics) of the main reservoir with the remaining oil; and Gupta et al. (2022), using the mathematical analysis of field recovery data, proposed a reliable, geoscience-driven technique for predicting residual oil zones (ROZ) development for the Wasson field case.

However, most existing results were derived from a single research program, which only explored mechanistic inferences, model building, and development phenomena, lacked a combined description of indoor experiments with field development, as well as a timeliness assessment approach for development scenarios (Nan 2021). Therefore, this paper takes well area X of the complex block reservoir at Tankou as the research object, systematically describes the current situation of water injection and development in this well area, and conducts quantitative research with the help of plate sand-filling experiments and numerical simulations. The goal is to explore the main control factors affecting the recovery rate without changing well network deployment and propose and verify development adjustment scenarios and the engineering verification method for the scenarios. This will help to explore the intrinsic causes of the disorder of injection and production coupling in the study area.

This study is intended to address the gap between engineering validation by bridging the results of conventional plate sand-filling experiments and numerical simulations. A well-matched, highly responsive, and mathematical analysis of the scheme analogy is proposed. It is expected to solve the problems of long validation cycles and weak parameter comparability, and to improve the systematic working steps of "experimentation → data simulation → proposal → mathematical demonstration" for reservoir development. The research problem is summarized as follows: (1) The effect of different permeability, crude oil viscosity, and recovery rate on the recovery rate under the premise of fixed well network is investigated through sand-filling experiments. (2) The effect of different crude oil viscosity, different recovery rate, and different permeability on the recovery rate is investigated through numerical simulation, and a graph and regression equation are derived. (3) The change in recovery rate before and after the implementation of the improved scheme is compared by a reliability analysis model, and the recovery rate is predicted by a discrete grey prediction model (DGM (1,1)).

Background and ideas

The Tankou oilfield, located in the eastern part of China, is a very complex block reservoir (Fig. 1). It is located in the Zhongtan fault zone, in the northern part of the Qianjiang depression within the Jianghan basin. The X well area, found within the eastern section of the Tankou oilfield, features a series of oil-bearing formations. These are primarily concentrated within the submerged 41, 41 lower, 40, 40 lower, 42, 43, and other oil groups. The oil reservoir burial depth extends from 660 to 2945 m, with a formation dip angle ranging from 45 to 60°. The average reservoir porosity is 23.8%, permeability measures at 534.2×10^{-3} μm^2, and surface crude oil density varies between 0.863 and 0.920 g/cm^3. Surface crude oil viscosity is 21.2–63.8 mPa s, original formation pressure is between 12.6 and 29.5 MPa, saturation pressure is 0.70–2.2 Mpa, and pressure coefficient is 1.12, classified as a medium pore medium permeability complexblock reservoir (Ma 2021). The area is characterized by a number of key geological features including the following: extremely developed low-sequence level faults, small fracture blocks, oil-bearing small layers with large differences in thickness and permeability, strong inter-stratigraphic inhomogeneity; complex oil-water relationships and large differences in natural energy. The area is largely laid out as an inverse nine-point well network, and the well locations are not indicated due to confidentiality of geological information (Liu et al. 2022).

The Tankou oilfield's X well area contains 38 oil wells and 7 water wells, which produce 77.6 tons of oil per day with an average production of 2.0 tons per well and a comprehensive water content of 53.0%. With a daily water injection of 139 m^3, 297×10^4 tons of oil have been recovered cumulatively up to now with a geological reserve recovery rate of 0.79% (calculated on the basis of recalculated reserves). The oil recovery rate is moderately low, with a current injection to recovery ratio of 0.85. The cumulative water recovery is 43×10^4 m^3, and the cumulative water injection is 16.8×10^4 m^3, with a cumulative injection ratio of 0.28. The formation deficit is severe, and the geological reserves recovery degree is low (8.9%). The current calibrated recovery rate is 15.04%, indicating large potential for development and adjustment to increase production. However, due to its complex geological structure, fluid

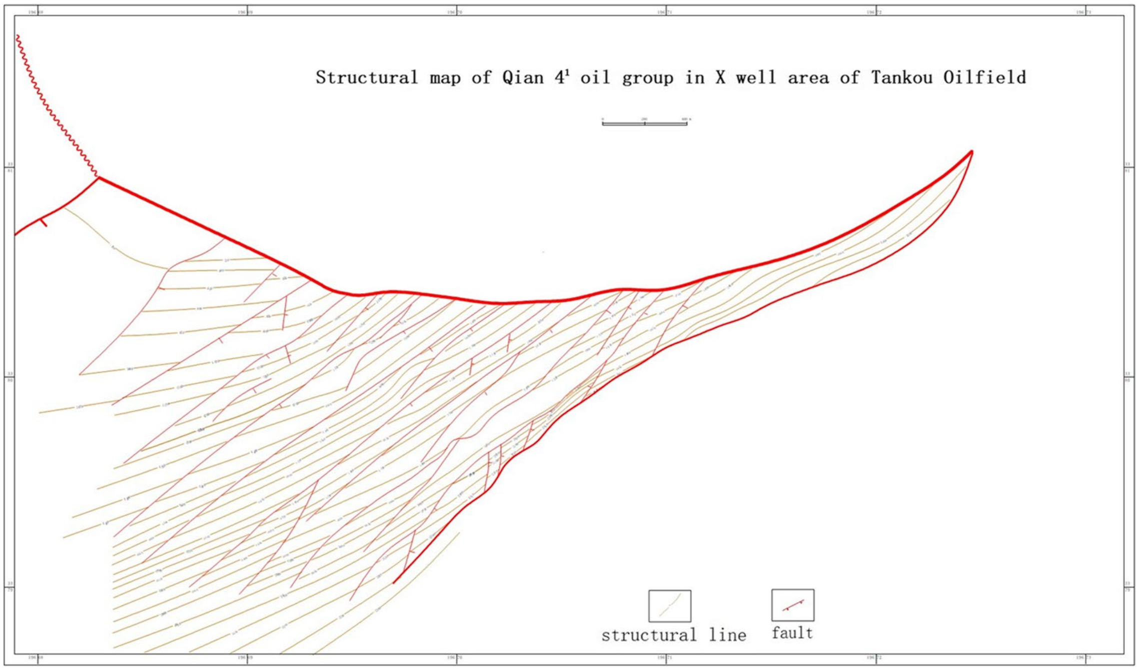

Fig. 1 Structural map of the top surface of submerged 41 in the western slope zone of the Tankou Bulge

properties, oil and water system, and special characteristics, it is necessary to conduct an experimental study on the physical modelling of water-driven oil plate for complex block reservoirs in order to formulate development adjustment measures for old oil areas that follow the principles of engineering-geology integration and optimize current development parameters to achieve stable production. The logic of this study is as follows (Fig. 2).

The first step of this study is to select the Tankou X well area as the research object and determine the experimental direction based on existing development data. The second step is to identify permeability, viscosity, and fluid extraction rate as the main factors influencing the current injection and extraction rate, and carry out sand-filling experiments and numerical simulation studies. The third step proposes a development adjustment plan based on the experimental results and carries out engineering verification with the help of a reliability analysis model. The fourth step selects final data from several observation points in the engineering verification for prediction.

Methodology

Three-dimensional physical simulation can better approximate real formation conditions, reflect heterogeneous changes in the reservoir during the water-driven oil process in both the longitudinal and lateral directions, and enable adjustment of the well network for the purpose of simulating reservoir development (Techarungruengsakul and Kangrang 2022). This experiment is based on the similarity criterion. By considering influencing factors such as permeability, crude oil viscosity, and fluid recovery rate, a three-dimensional physical simulation of water-driven oil flat sand filling experiment is carried out to explore the main controlling factors affecting the recovery rate and provide a basis for improving the reservoir development effect in well area X of the Tankou oilfield. As the well network deployment in the study area has been determined, we do not explore the effect of well network density here. The experimental conditions are set as the inverse nine-point well network closest to the field working conditions. The fitted equation for the bound water saturation in this work area is $S_{wi} = 121.27e^{-0.1685\varphi}$. The experimental setup and flow chart are shown in Fig. 3.

Materials and equipment The constant velocity displacement pump has a flow rate range of 0.001~200 mL/min and a pressure resistance of 5 MPa. The piston-type intermediate vessel was used, along with a pressure gauge and flat plate model (size, 30 × 30 × 5 cm; various combinations of well networks such as the four-point well network, five-point well network, seven-point well network, and nine-point well network could be achieved by adjusting the well network arrangement on the main body of the model). The measuring cylinder and six-way valve were also used.

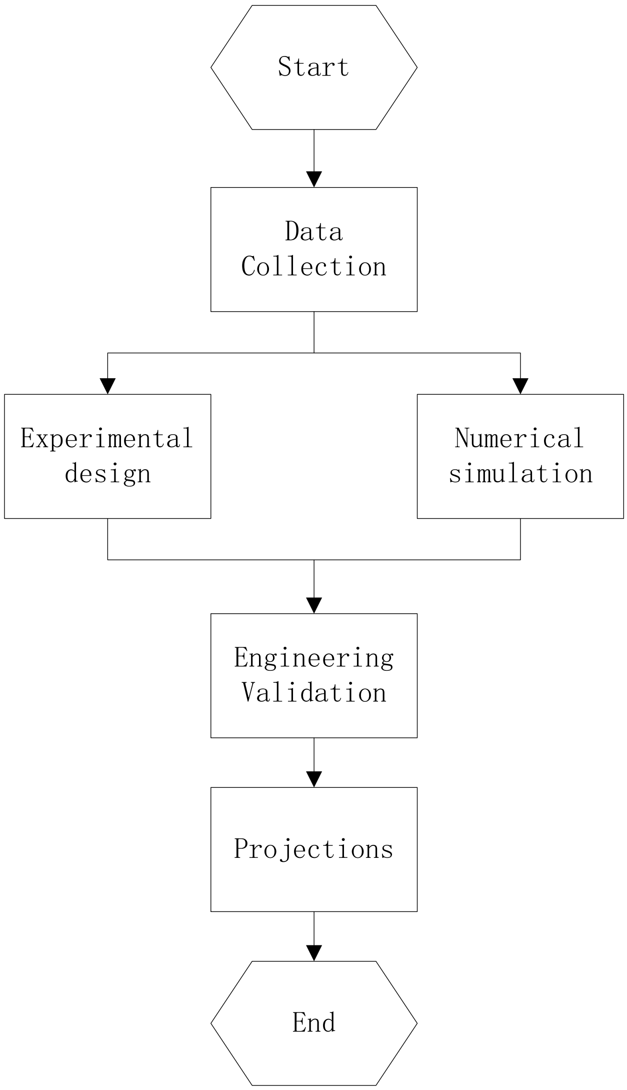

Fig. 2 Research logic diagram

Experimental samples Stratigraphic water samples, stratigraphic crude oil samples, and quartz sand of different mesh sizes were used.

Experimental steps for different permeability conditions The experimental setup was assembled, and a flat plate model with permeability x and well spacing of 12 cm was filled with quartz sand of different mesh sizes. The filled model was injected with formation water, and then an inverse nine-point well network with saturated 180 mPa s formation crude oil was simulated. The water drive experiment was conducted at a flow rate of 2 mL/min. The experiment was terminated when the integrated water content of the recovery well reached 98%. The recovery rates were measured for two cases of 1000 mD and 2000 mD permeability of the plate-physical model experimental bench, respectively, and the recovery rate versus time curve was plotted for each well.

The experimental protocol for investigating crude oil viscosities The experimental rig was configured, and a flat plate model with a permeability of 2000 mD and a well spacing of 12 cm was packed with quartz sand of various mesh sizes. Subsequently, the filled model was first flushed with formation water, and the formation water was then replaced with crude oil of a viscosity x. Finally, the bound water saturation was adjusted to approximately 39% by means of an equation. The injection line was connected using the inverse nine-point well network access method, and the formation water was injected at a constant rate of 2 mL/min. The experiment was terminated when the integrated water content of the recovered wells reached 98%. The recovery rates were measured for the viscosity cases of 90, 180, and 360 mPa s viscosity, and the recovery rate over time was plotted for each well.

Experimental protocol for varying fluid recovery rates (1) The experimental rig was assembled and a flat plate model with a permeability of 2000 mD and a well spacing of 12 cm was filled with quartz sand of various mesh sizes. (2) The filled model was injected with formation water, and then the inverse nine-point well network was simulated with formation crude oil of viscosity 180 mPa s, and water drive experiments were conducted at a flow rate of x. (3) The experiment was terminated when the integrated water content of the recovered wells reached 98%. (4) The recovery rate was measured for three cases of recovery rate of 1 mL/min, 2 mL/min, and 5 mL/min, respectively, and the recovery rate over time curve was plotted for each well.

Numerical simulation method The effect of different crude oil viscosities, different recovery rates, and different permeabilities on the recovery rate was simulated using Petrel RE software. A graph of the effect of different factors on water-driven oil and the regression equation were obtained (Wali and Baqer 2020). The mechanism model used a 30 × 30 × 1 grid system with a grid size of 1 cm × 1 cm in the plane and one simulation layer in the vertical direction according to the variable depth, with a single layer grid thickness of 5 cm. The total number of nodes in the model was 30 × 30 × 1 = 900. There were 16 wells in the model, which were set to the nine-point method by switching wells. The crude oil viscosity was set at 90, 180, 270, and 360 mPa s; the permeability was set at 500, 1000, 1500, 2000, 2500, and 3000 mD; and the fluid recovery rate was set at 1, 2, 3, 4, and 5 mL/min (Figs. 4 and 5).

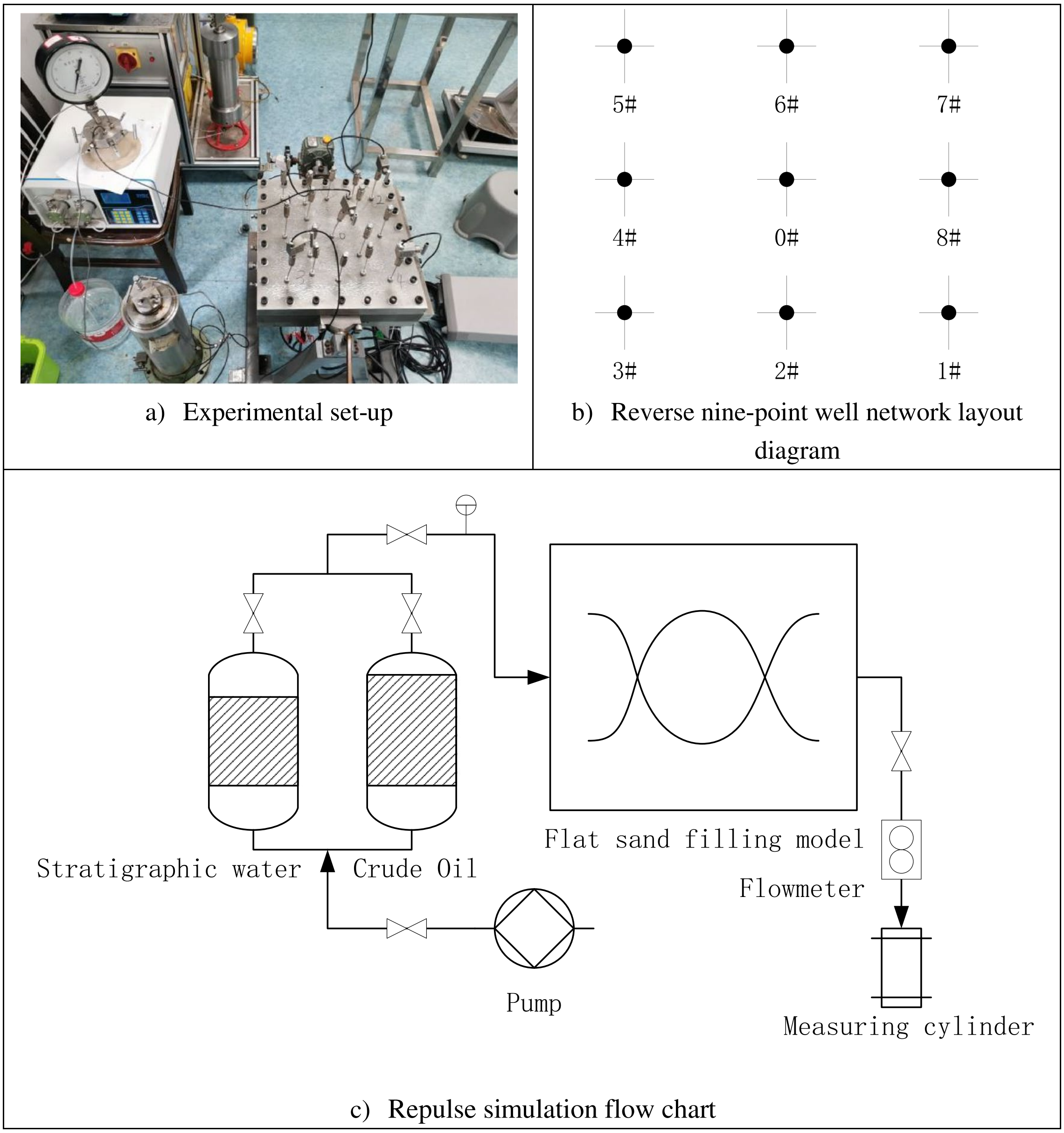

a) Experimental set-up
b) Reverse nine-point well network layout diagram
c) Repulse simulation flow chart

Fig. 3 Experimental setup and flow chart

Experimental analysis

Influence of permeability

Numerical simulation approach The impact of various crude oil viscosities, recovery rates, and permeabilities on the recovery rate was simulated using the Petrel RE software package. A graph depicting the influence of various factors on water-driven oil and the corresponding regression equation was obtained (Wali and Baqer 2020). There were 16 wells present in the model, which were arranged in a nine-point configuration by switching wells.

The final recovery rates of wells 1#, 3#, 5#, and 7#, which are located further away from the injection well 0#, were higher than those of wells 2#, 4#, 6#, and 8#, which are located closer when the permeability, crude oil viscosity, and fluid extraction rate were different. The recovery rates in the two subgroups were ranked as follows: 1# > 3# > 7# > 5#; and 2# > 8# > 6# > 4#. These three factors were determined experimentally. Experimental measurements of the three influencing factors indicated that 3000 min was the optimal period for stable production. The steady production period can be extended to 5000 min when the recovery rate reaches 1 mL/min or the crude oil viscosity is 360 mPa s.

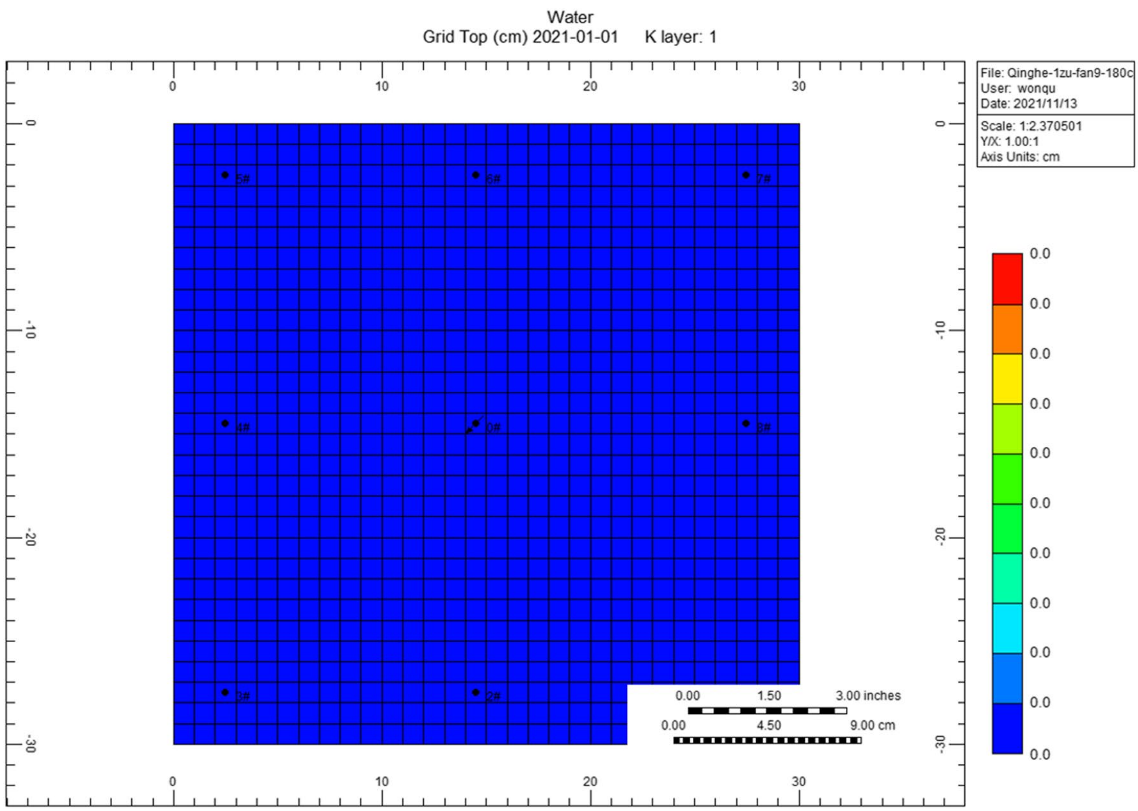

Fig. 4 Planar grid diagram of the flat plate mechanism model (plane)

In the experiments on the influence of permeability (Figs. 6 and 7), the development curves of the two subgroups started to separate at different times: 119 min and 250 min for the permeability values of 1000 mD and 2000 mD, respectively. The curves showed a rapid upward trend at 250 min. The initial recovery increase was greater for the premise with a permeability value of 1000 mD compared to that with a permeability value of 2000 mD, which may be due to the fact that a flow rate of 2 mL/min can adequately overcome the capillary force in the pore space at the early stage of injection and recovery, and the hydraulic agitation effect in the smaller permeability environment can promote crude oil replacement in a limited time.

Viscosity effects

A total oil content of 1108 mL was obtained for a simulated pore volume of 1830 cm^3 with a crude oil viscosity of 90 mPa s. The cumulative oil production was 516.90 mL, resulting in a calculated final recovery rate of 46.65%. When the crude oil viscosity was 180 mPa s and the simulated pore volume was 1830 cm^3, the total oil content was 1103.35 mL. The cumulative oil production was 489.9 mL, leading to a calculated final recovery rate of 44.40%. When the crude oil viscosity was 360 mPa s and the experimental simulation pore volume was 1830 cm^3, the total oil content was 1094.45 mL. The cumulative oil production was 469.30 mL, resulting in a calculated final recovery rate of 42.88%. Separate recovery rate versus time curves were plotted (Figs. 8, 9, and 10).

Viscosity effects in the experiments (Figs. 8, 9, and 10). Firstly, wells 1#, 3#, 5#, and 7#, which are farther away from the injection wells in a straight line, and wells 2#, 4#, 6#, and 8#, which are closer to the injection wells in a straight line, show a typical rise in separation at 100–200 min. The recovery rise and final value of the wells which are farther away from the injection wells in a straight line are larger, so the recovery rate can be improved when the well spacing reaches a certain value (Gao, et al. 2020). In addition, the curve for well #1 developed in a stepwise manner between about 1600 to about 180 min after well #9 had developed between about this time had started developing strongly with the rate began developing wells #3, #5, and #7.

This may be due to the influence of the plastic state of the crude oil, which is more active at viscous flow temperatures in this environment at the 90 mPa s premise, resulting in viscoelastic transition zone transitions in the material properties themselves and hydraulic flushing leading to recovery fluctuations. At the 360 mPa s high viscosity premise, there are greater molecular forces on the oil droplets, which are more

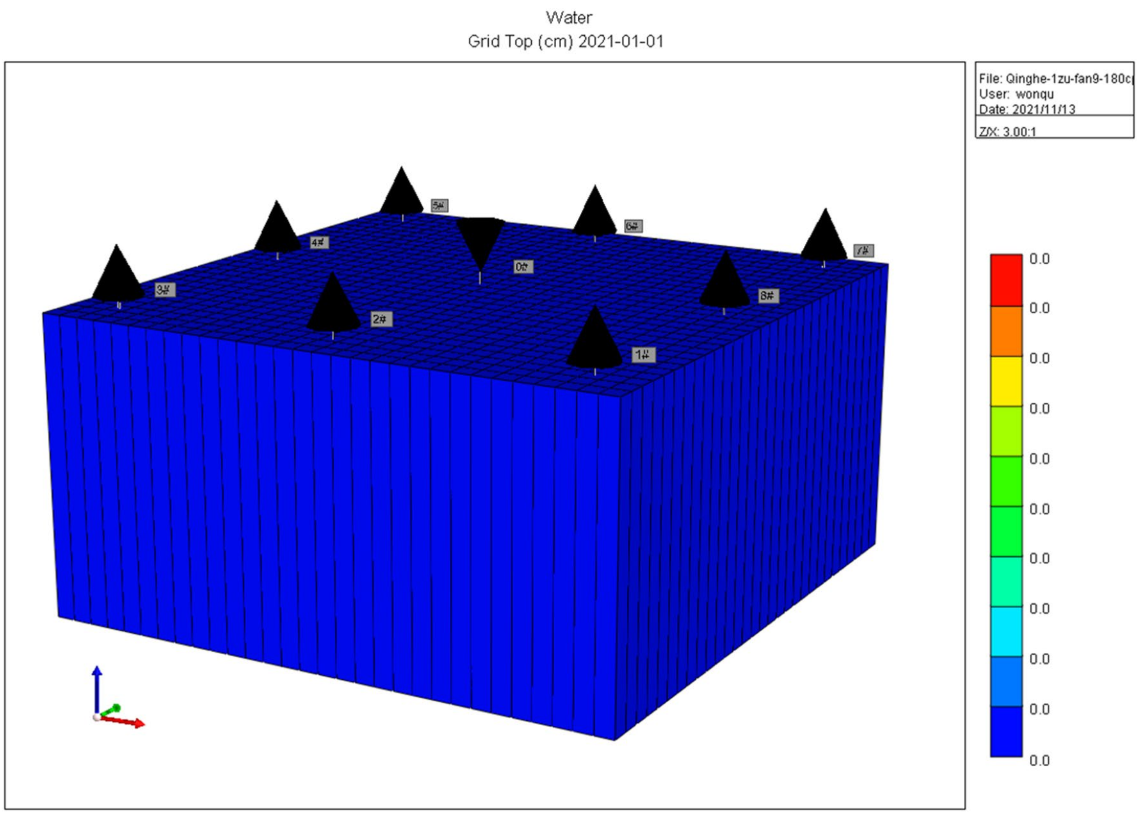

Fig. 5 Profile grid view of the flat plate mechanism model (3D)

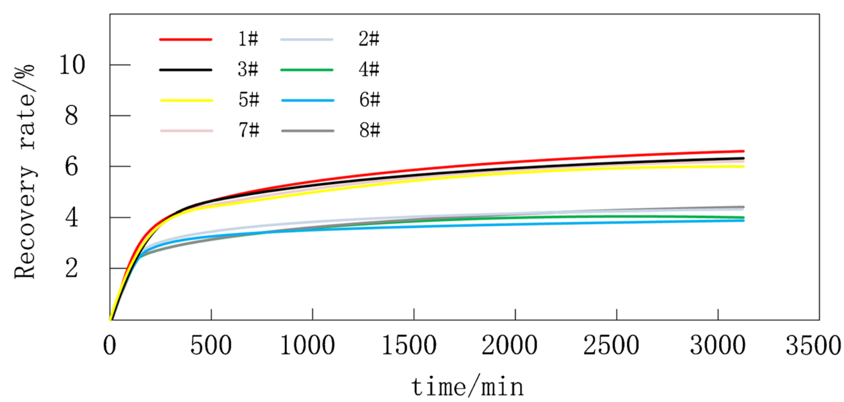

Fig. 6 Recovery rate versus time for each well at 1000 mD

likely to be aggregated and recovered by water displacement (Wang et al. 2017).

Influence of fluid extraction rate

The experimentally simulated pore volume was 1830 cm^3 with an extraction rate of 1 mL/min, and the total oil content was 1100 mL. This cumulative oil production was 463.90 mL, resulting in a calculated final recovery of 42.17%. When the fluid extraction rate was 2 mL/min, the experimentally simulated pore volume was 1830 cm^3 and the total oil content was 1103.35 mL. This cumulative oil production was 489.9 mL, leading to a calculated final recovery of 44.40%. When the fluid extraction rate was 5 mL/min, the experiment

Fig. 7 Recovery rate versus time for each well at 2000 mD premise

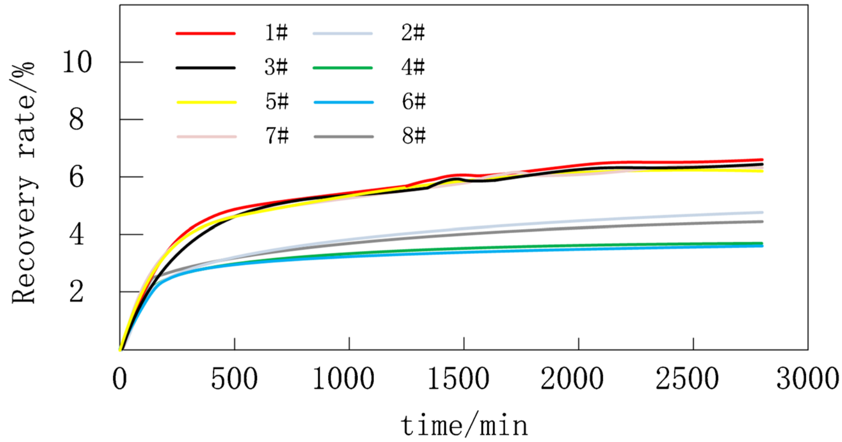

Fig. 8 Recovery rate versus time for each well at crude oil viscosity 90 mPa s

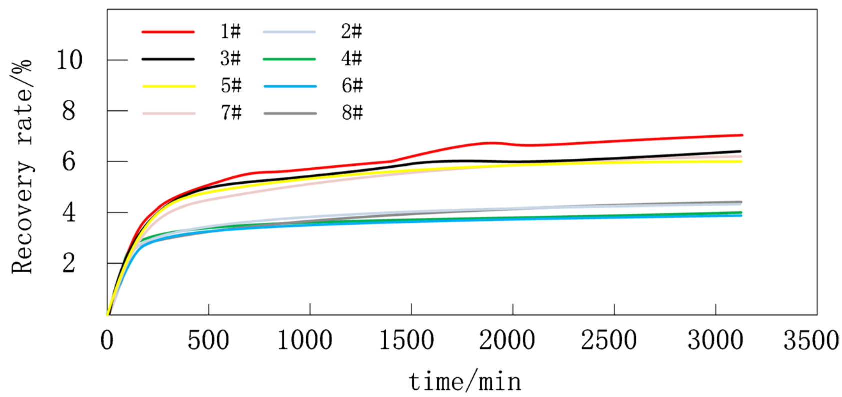

Fig. 9 Recovery rate versus time for each well at crude oil viscosity 180 mPa s

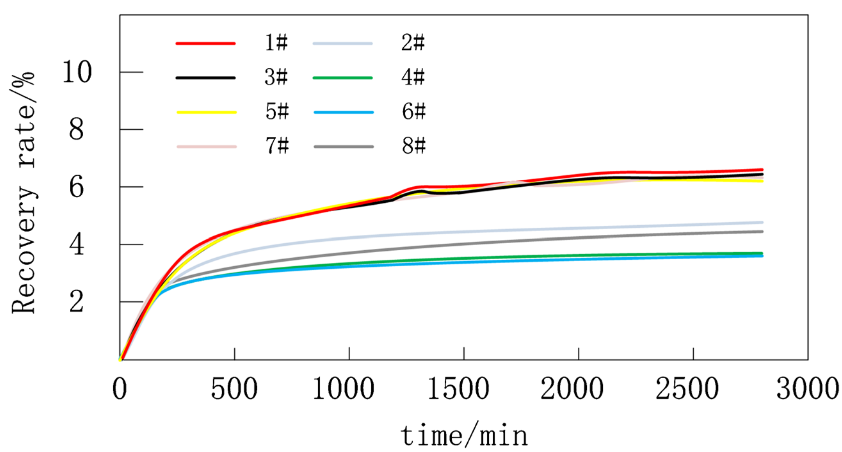

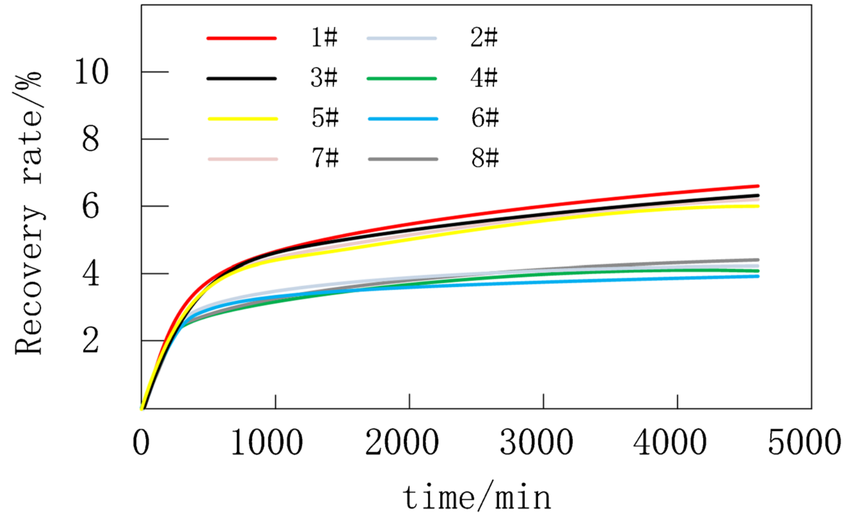

Fig. 10 Recovery rate versus time for each well at crude oil viscosity 360 mPa s

simulated a pore volume of 1830 cm^3 and a total oil content of 1102 mL. The cumulative oil production was 528.1 mL, resulting in a calculated final recovery of 47.92%. Separate recovery rate versus time curves were plotted (Figs. 11, 12, and 13).

In the experiments on the effect fluid production rate (Figs. 11, 12, and 13), at the 1 mL/min, 2 mL/min, and 5 mL/min premise, the development curves of the two subgroups started to separate when the experiments were conducted to 50 min, 40 min, and 30 min, respectively. The well development curves for the 5 mL/min premise show a balanced separation trend and the greatest initial curve slope. This may be due to the higher flow rate generating a stronger repelling force and more complete repelling of the crude oil in the pore space.

Under the same permeability, well network, and fluid extraction rate conditions, the recovery rate gradually decreases with increasing crude oil viscosity, showing a power decreasing trend. The recovery rate increases gradually with increasing fluid extraction rate under the same permeability, crude oil viscosity, and well network conditions, with a multiplying power increasing trend; The recovery rate for a permeability of 1000 mD is 1.76% lower than the recovery rate of the flat plate model of 2000 mD for the same crude oil viscosity, well network, and fluid recovery rate conditions.

Summary of fluid production and oil production data

The measured data from the different experimental categories were screened to compare the last set of individual well production data at the end of the water-driven oil experiment (Table 1). It can be seen that the recovery wells close to the relative water injection wells produced high fluid volumes but low oil production. However, a comprehensive comparison of the average oil recovery, fluid recovery, and recovery rates under different conditions is also required.

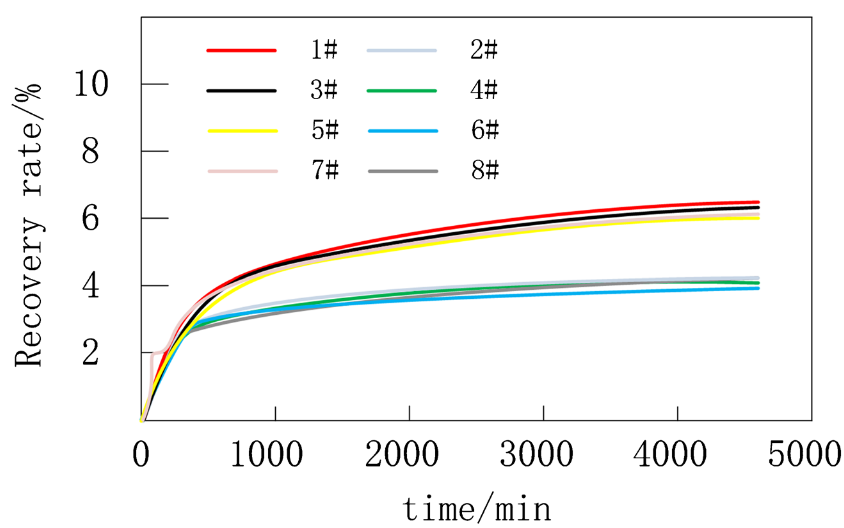

Fig. 11 Recovery rate versus time for each well at 1 mL/min

Fig. 12 Recovery rate versus time for each well at 2 mL/min

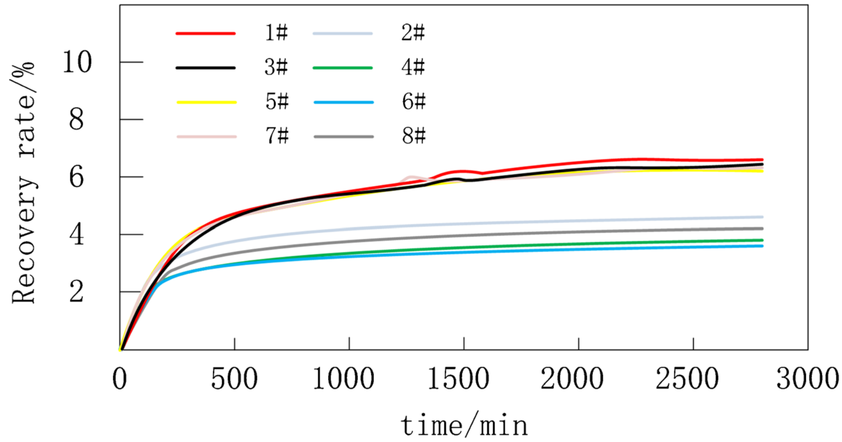

Fig. 13 Recovery rate versus time for each well at 5 mL/min

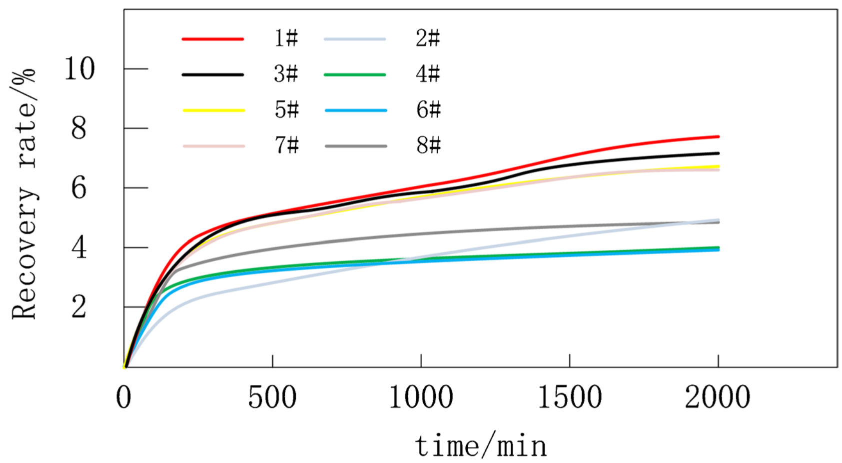

Numerical simulation

The findings from the flat plate experiments can be further extended through numerical simulations. The data fitting curve can produce a realistic and reliable relationship equation, which can be easily called during the mining process.

A comparison between the numerical simulation and experimental results of viscosity influencing factors shows that the inverse recovery closely resembles the experimental recovery and meets the research needs. As the viscosity of the crude oil increases, the recovery rate tends to decrease exponentially. The numerical simulation inversion fitting relationship equation is $y = 65.451x^{-0.0695}$.

A numerical simulation of the influencing factors of the recovery rate and a comparison of the experimental results show that the inverse recovery rate is generally consistent with the experimental recovery rate and meets the research requirements. As the recovery rate increases, the recovery rate gradually rises, following a logarithmic trend. The numerical simulation inversion fitting equation is $y = 3.0698\ln(x) + 43.503$.

A numerical simulation of the influencing factors of permeability and a comparison of the experimental results show that the inverse recovery rate is generally consistent with the experimental recovery rate and meets the research requirements. As the permeability of the model increases, the recovery rate gradually rises, following a polynomial trend. The numerical simulation inversion fitting equation is $y = 18.898x^{0.1173}$.

In summary, the numerical simulation inversion fitting relationship curve and the experimental data curve of the sand-filled plate are generally in agreement with each other, and the difference in the R-value is small. Therefore, the relationship equation is valid (Figs. 14, 15, and 16).

Table 1 Table of results of water-driven oil experiments

Conditions	Closing time, min	Volume of liquid produced, mL	Oil production, mL	Volume of liquid produced, mL	Oil production, mL	Volume of liquid produced, mL	Oil production, mL	Volume of liquid produced, mL	Oil production, mL	Volume of liquid produced, mL	Oil production, mL	Volume of liquid produced, mL	Oil production, mL	Volume of liquid produced, mL	Oil production, mL	Volume of liquid produced, mL	Oil production, mL	Recovery rate, %
		1#Oil well		2#Oil well		3#Oil well		4#Oil well		5#Oil well		6#Oil well		7#Oil well		8#Oil well		
1000 mD permeability	3060	419	61	988.5	44.1	468	57.1	1131.5	42.3	524	56.5	1131.5	41.8	469	57.5	988.5	46.2	42.64
2000 mD permeability	2675	382.5	72.5	851	57	425	71.3	969.9	48.4	475.5	68.6	969	48.3	425.5	70.1	851	53.7	44.4
90 mPa s viscosity	2970	471	81.8	920	54.7	514	75.7	1023	50.1	561.6	73.7	1023	50.6	513	75.5	918.1	54.8	46.65
180 mPa s viscosity	2675	382.5	72.5	851	57	425	71.3	969.9	48.4	475.5	68.6	969	48.3	425.5	70.1	851	53.7	44.40
360 mPa s viscosity	4320	603	70.2	1375.5	52.7	678.6	66.3	1581.5	48.1	765.5	64.2	1582	48.4	677.5	66.1	1375.5	53.3	42.88
1 mL/min fluid collection speed	4450	310.5	72	713.5	49.9	346.5	67.5	815.5	46	388.5	65.4	815.5	46.1	348.8	67.5	713	49.5	42.17
2 mL/min fluid collection speed	2675	382.5	72.5	851	57	425	71.3	969.9	48.4	475.5	68.6	969	48.3	425.5	70.1	851	53.7	44.4
5 mL/min fluid collection speed	1860	713	81.5	1447	60.3	785	76.7	1627	50.2	867	72.3	1630	50.3	787	76.7	1480	60.1	47.92

Engineering verification and project prediction

Engineering validation

Conventional oil recovery program validation is typically based on recovery rates and well maintenance frequency over a period of 1 year or longer, resulting in long validation cycles and high economic costs. Therefore, accelerated experiments are necessary to verify the feasibility of adjustment schemes (Escobar and Meeker 2006). Here, we have selected the reliability analysis approach from quality engineering, focusing on internal and external factors that lead to weaknesses, identifying patterns, recommending improvement measures, and the impact of those improvements on system reliability.

The engineering validation method involves performing a reliability analysis using Minitab software with reliability as the determination indicator. The model steps are:

(1) Data screening

Based on the requirements of the distribution analysis arbitrary deletion function module, a maximum of 50 columns of sample data containing start times were entered into the initial and ending variables. The start time in this column depends on how the data is censored. A column containing the failure mode was entered. Representation of right-censored observations in the failure mode column (Kalpande and Toke 2022).

(2) Data fit and goodness-of-fit test

The failure mode data column will follow the Weibull distribution model, the exponential distribution model, the extreme value distribution model, and the normal distribution model. The goodness-of-fit test for the full data column is usually performed using maximum likelihood, the chi-square test, and least squares function (Galetto 2022). The chi-square test is calculated as:

$$\chi^2 = \sum_{i=1}^{k} \frac{(f_{oi} - f_{ei})^2}{f_{ei}} \tag{1}$$

where χ^2 is the chi-square test; f_{oi} is the observed frequency in group i; f_{ei} is the expected frequency in group i; k is the number of data sets.

For the exponential distribution, the maximum likelihood estimate for parameter λ is

$$\hat{\lambda} = n / \sum_{i=1}^{n} t_i \tag{2}$$

The maximum likelihood estimate for μ and σ^2 in the normal distribution is

$$\hat{\mu} = \bar{x} = \frac{1}{n} \sum_{i=1}^{n} x_i \tag{3}$$

$$\hat{\sigma}^2 = \frac{1}{n} \sum_{i=1}^{n} (x_i - \bar{x})^2 \tag{4}$$

For the log-normal distribution, the maximum likelihood estimates of μ and σ^2 can be obtained from the parameter estimates of the normal distribution as

$$\hat{\mu} = \frac{1}{n} \sum_{i=1}^{n} \ln x_i \tag{5}$$

$$\hat{\sigma}^2 = \frac{1}{n} \sum_{i=1}^{n} [\ln x_i - \frac{1}{n} \sum_{i=1}^{n} \ln x_i]^2 \tag{6}$$

For the two-parameter Weibull distribution, the maximum likelihood estimate of its parameters is solved iteratively by the following transcendental equation:

$$\left\{ \begin{array}{c} \frac{\sum_{i=1}^{n} x_i^{\beta} \ln x_i}{\sum_{i=1}^{n} x_i^{\beta}} - \frac{1}{\beta} - \frac{1}{n} \sum_{i=1}^{n} \ln x_i = 0 \\ \eta^{\beta} = \frac{1}{n} \sum_{i=1}^{n} \end{array} \right\} \tag{7}$$

The parameters to be estimated in the initially selected distribution model are specifically the parameters of the exponential distribution λ, the mean μ and standard deviation σ of the normal distribution, the log mean μ and log standard deviation σ of the lognormal distribution, and the scale parameter η and shape parameter β of the two-parameter Weibull distribution (Shitana and Michael 2022; Abdelfattah et al. 2022).

(3) Hypothesis testing and reliability calculations

The two-parameter Weibull distribution is usually preferred in the calculation (Wang et al. 2023a, b). Therefore, using the Weibull distribution as an example, write the failure distribution function $F(t)$ and the reliability function $R(t)$ for the two-parameter Weibull distribution as follows:

$$F(t) = 1 - \exp[-(\frac{t-\gamma}{\eta})^{\beta}] \tag{8}$$

$$R(t) = \exp[-(\frac{t-\gamma}{\eta})^{\beta}] \tag{9}$$

where η is the scale parameter; β is the shape parameter; γ is the threshold parameter.

Based on the recovery statistics of 38 existing wells in the study area and the conclusions of the sand-filling

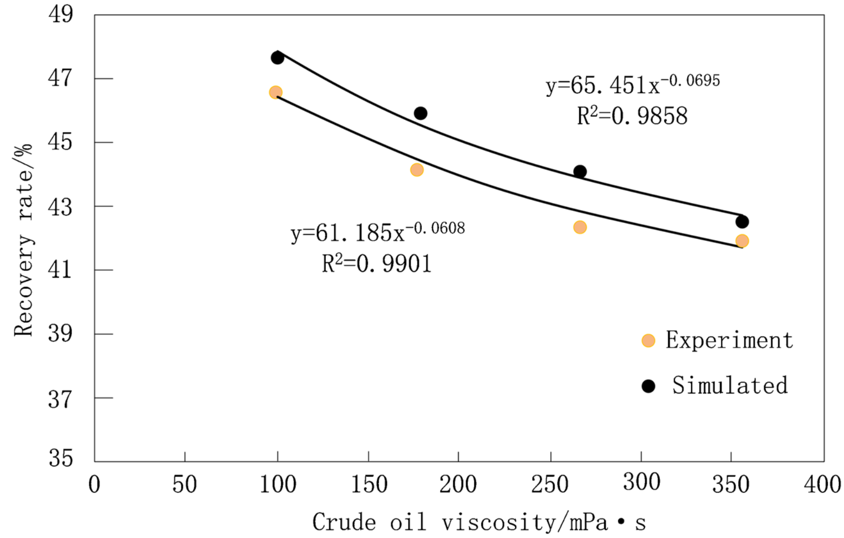

Fig. 14 Curve of the effect of crude oil viscosity on the effect of water on oil drive

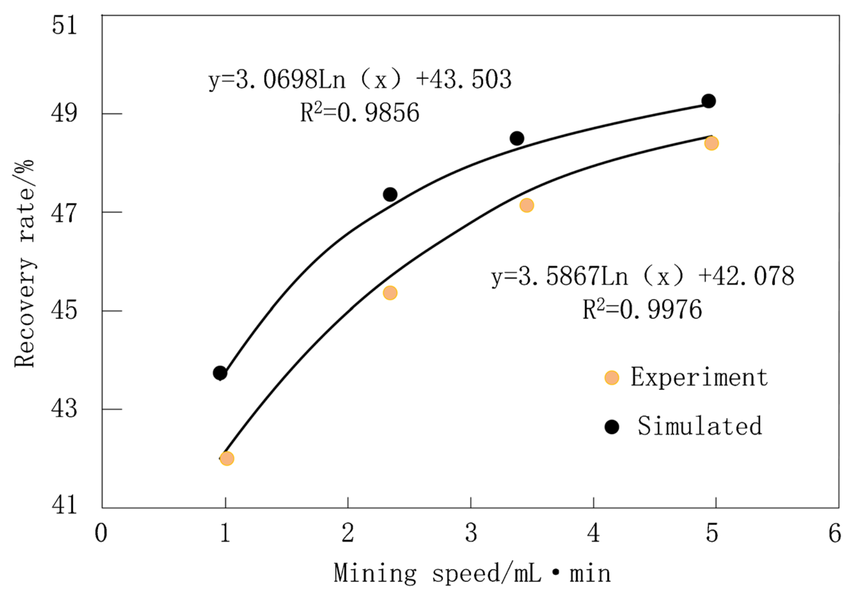

Fig. 15 Curve of the effect of fluid recovery rate on the effect of water on oil drive

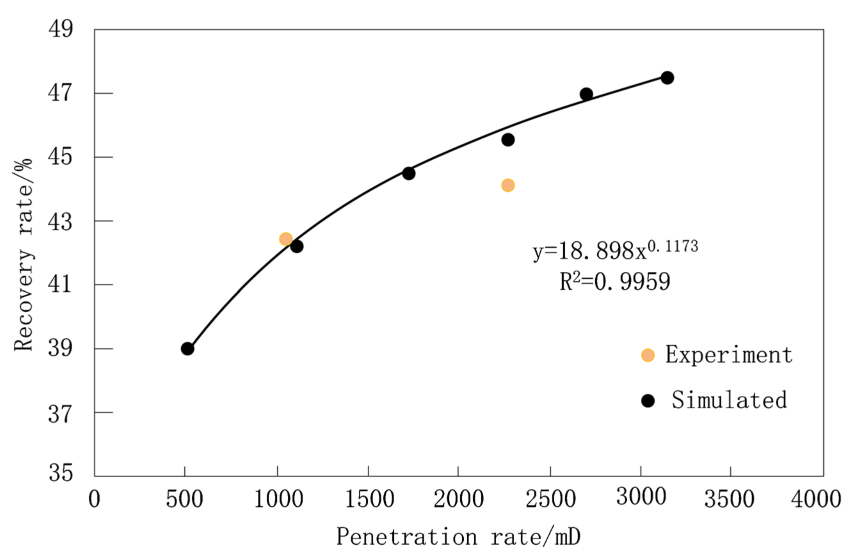

Fig. 16 Curve of the effect of model permeability on the effect of water on oil drive

experiments on the flat plate, the moderate recovery rate, derived from the preconditions of 2000 mD permeability, 180 mPa s viscosity, and 2 mL/min fluid recovery rate, was taken and averaged. The real 15.04% calibration recovery rate for the study area was then compared. It was determined that there was an error between the plate sand-filling experiment and the real working conditions, so a 3-fold year-on-year reduction was taken to weaken the error and arrive at a threshold of 14.8%. A single well recovery rate of less than 4.8% was considered to be a failure, and the frequency of failures was calculated for each 3-week interval for 53 weeks before and after the implementation of the adjustment program for X wells in the study area (Table 2). Reliability analysis was performed using Minitab software with arbitrary deletions. The reliability was compared before and after the implementation of the program.

A goodness-of-fit test based on the maximum likelihood function showed that the full data columns were consistent with an exponential distribution. Additionally, the parametric distribution analysis produced an exponential probability plot for scenario comparison at a 95% confidence level (Fig. 17), as well as the percentiles of the exponential distribution before and after scenario execution (Table 3).

The above calculations demonstrate that the mean estimate before the program was 25.7081, with 99% of the wells having a life expectancy greater than 0.258375 at the preset recovery threshold, and the mean estimate after the program was 27.5591, with 99% of the wells having a life expectancy greater than 0.276978 at the preset recovery threshold. The combined well life expectancy after program implementation exceeded that before implementation. Although the technical life data was not significantly higher, the engineering reality that the new program can only slightly improve recovery after implementation was reinforced. This confirms the effectiveness of the program.

Development program forecast

The recovery data from the end observation points after the implementation of the new program were collected and combined with the requirement that the DGM (1,1) model calculation requires at least four data sets and that the modelled data cannot be zero. The data strings 2, 3, 4, 1, 12, and 9 were selected, and the large fluctuation point 12 was manually excluded.

The prediction method selected was the grey system DGM (1,1) model, operating in a time-varying functional framework, which requires a minimum of four sets of time series data. Firstly, stochastic perturbation weakening was applied, raw data was cumulatively transformed, then a least squares exponential fit curve was operated to achieve functional prediction, and finally residual detection was applied to test the confidence of the results (Wang et al. 2020; Ye et al. 2019; Zhao et al. 2018). Model steps:

(1) Let the time series $X^{(0)}$ have n observations, $X^{(0)} = \{x^{(0)}(1), x^{(0)}(2), x^{(0)}(3) \cdots x^{(0)}(n)\}$, and generate a new series by accumulating once:

$$X^{(1)} = \{x^{(1)}(1), x^{(1)}(2), x^{(1)}(3) \cdots x^{(1)}(n)\} \tag{10}$$

(2) Generate the DGM (1,1) model differential equation:

$$x^{(1)}(k+1) = \beta_1 x^{(1)}(k) + \beta_2 \tag{11}$$

where $x^{(1)}(k) = \sum_{i=1}^{k} x^{(0)}(i), k = 1,2, \cdots, n$;

$$\begin{cases} \beta_1 = \dfrac{\sum_{i=1}^{n-1} x^{(1)}(i+1)x^{(1)}(i) - \frac{1}{n-1}\sum_{i=1}^{n-1} x^{(1)}(i+1)\sum_{i=1}^{n-1} x^{(1)}(i)}{\sum_{i=1}^{n-1} (x^{(1)}(i))^2 - \frac{1}{n-1}(\sum_{i=1}^{n-1} x^{(1)}(i))^2} \\ \beta_2 = \frac{1}{n-1}\left[\sum_{i=1}^{n-1} x^{(1)}(i+1) - \beta_1 \sum_{i=1}^{n-1} x^{(1)}(i)\right] \end{cases} \tag{12}$$

(3) Apply least squares to calculate parameter values:

If $\widehat{\beta} = (\beta_1, \beta_2)^T$ is a parametric column and

$$B = \begin{pmatrix} X^{(1)}(1) & 1 \\ X^{(1)}(2) & 1 \\ \cdots & \\ X^{(1)}(n-1) & 1 \end{pmatrix}, Y = \begin{pmatrix} X^{(1)}(2) \\ X^{(1)}(3) \\ \cdots \\ X^{(1)}(n) \end{pmatrix} \tag{13}$$

Table 2 Failed sample data statistics

Start (old), week	End (old), week	Frequency (old), times	Start (new), week	End (new), week	Frequency (new), times
	3	0		3	1
3	6	1	3	6	0
6	9	23	6	9	3
9	12	17	9	12	11
12	15	20	12	15	12
15	18	3	15	18	8
18	21	10	18	21	9
21	24	19	21	24	5
24	27	22	24	27	4
27	30	2	27	30	7
30	33	7	30	33	8
33	36	9	33	36	0
36	39	16	36	39	2
39	41	3	39	41	3
41	44	23	41	44	4
44	47	11	44	47	1
47	50	4	47	50	12
50	53	2	50	53	9

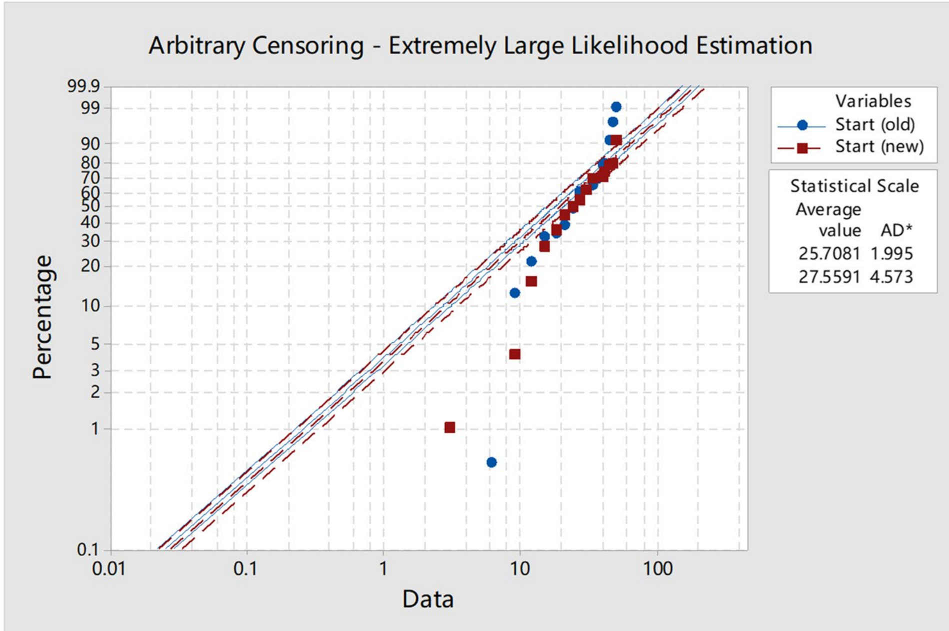

Fig. 17 Probability plot of exponential distribution for comparison of scenarios with 95% confidence level

Table 3 Percentile distribution of indices before and after program implementation

Percentage	Before program implementation				After program implementation			
	Percentile	Standard error	Lower limit	Upper limit	Percentile	Standard error	Lower limit	Upper limit
1	0.258375	0.0186571	0.224277	0.297656	0.276978	0.0278509	0.227434	0.337315
2	0.519373	0.0375036	0.450831	0.598334	0.556769	0.0559845	0.457177	0.678055
3	0.783047	0.0565434	0.679709	0.902096	0.839429	0.0844067	0.689276	1.02229
4	1.04945	0.0757805	0.910959	1.20901	1.12502	0.113123	0.923781	1.37009
5	1.31865	0.095219	1.14463	1.51913	1.4136	0.142141	1.16074	1.72154
6	1.5907	0.114863	1.38077	1.83253	1.70523	0.171465	1.40021	2.0767
7	1.86565	0.134718	1.61944	2.14929	1.99998	0.201103	1.64224	2.43566
8	2.14358	0.154787	1.86069	2.46947	2.29792	0.231062	1.88688	2.7985
9	2.42455	0.175075	2.10458	2.79315	2.59912	0.261348	2.1342	3.16531
10	2.70862	0.195587	2.35116	3.12041	2.90364	0.291969	2.38425	3.53617
20	5.73659	0.414236	4.97954	6.60874	6.14964	0.618362	5.04962	7.48928
30	9.16942	0.662118	7.95934	10.5635	9.82964	0.988396	8.07137	11.9709
40	13.1323	0.948278	11.3993	15.1289	14.0779	1.41557	11.5597	17.1446
50	17.8195	1.28673	15.4679	20.5286	19.1025	1.92081	15.6856	23.2638
60	23.5561	1.70097	20.4474	27.1373	25.2522	2.53917	20.7352	30.7531
70	30.9518	2.23501	26.8671	35.6575	33.1804	3.33638	27.2453	40.4085
80	41.3755	2.9877	35.9152	47.666	44.3547	4.45998	36.4207	54.0169
90	59.195	4.27444	51.3831	68.1946	63.4572	6.38078	52.1063	77.2808
91	61.9036	4.47002	53.7343	71.315	66.3608	6.67275	54.4906	80.8169
92	64.9316	4.68867	56.3626	74.8033	69.6068	6.99915	57.1559	84.77
93	68.3644	4.93655	59.3424	78.758	73.2868	7.36918	60.1777	89.2517
94	72.3273	5.22271	62.7824	83.3235	77.5351	7.79635	63.666	94.4254
95	77.0145	5.56117	66.851	88.7232	82.5597	8.30159	67.7919	100.545
96	82.7511	5.9754	71.8305	95.3319	88.7093	8.91995	72.8415	108.034
97	90.1468	6.50945	78.2502	103.852	96.6376	9.71716	79.3516	117.689
98	100.571	7.26214	87.2984	115.861	107.812	10.8408	88.5271	131.298
99	118.39	8.54887	102.766	136.389	126.914	12.7616	104.213	154.562

Then the series of least squares estimated parameters for the discrete grey forecasting model $X^{(1)}(k+1) = \beta_1, X^{(1)}(k) + \beta_2$ satisfies:

$$\hat{\beta} = (\beta_1, \beta_2)^T = (B^T B)^{-1} B^T Y \tag{14}$$

(4) Taking $X^{(1)}(1) = X^{(0)}(1)$, the recursive function is

$$\hat{X}^{(1)}(k+1) = \beta_1^k X^{(0)}(1) + \frac{1-\beta_1^k}{1-\beta_1} \times \beta_2 \text{ or } \hat{X}^{(1)}(k+1) = \beta_1^k (X^{(0)}(1) - \frac{\beta_2}{1-\beta_1}) + \frac{\beta_2}{1-\beta_1} \tag{15}$$

(5) Discrete solver prediction model:

$$\hat{X}^{(0)}(k+1) = \hat{X}^{(1)}(k+1) - \hat{X}^{(1)}(k) \tag{16}$$

(6) Residual tests are carried out to calculate $\hat{X}^{(1)}(i)$ according to the prediction model, and $\hat{X}^{(1)}(i)$ is accumulated to generate $\hat{X}^{(0)}(i)$. The absolute and relative error series of the original series $X^{(0)}(i)$ and $\hat{X}^{(0)}(i)$ are then calculated as follows:

$$\Delta^{(0)}(i) = X^{(0)}(i) - \hat{X}^{(0)}(i) \tag{17}$$

where $i = 1, 2..., n$

$$\Phi(i) = \frac{\Delta^{(0)}(i)}{X^{(0)}(i)} \times 100\% \tag{18}$$

where $i = 1, 2 \cdots, n$

The calculation process is as follows:

(1) Initialization of the original sequence: 2, 3, 4, 1, 9
(2) 1-AGO generation of the original series: 2.0000, 5.0000, 9.0000, 10.0000, 19.0000.
(3) Calculation of the grey model development coefficient a and the grey action volume b: $a = 1.3537$; $b = 1.9512$
(4) Calculation of simulation values: 2.0000, 2.6585, 3.5988, 4.8715, 6.5943
(5) Residuals, 21.0532; mean relative error, 34.9868%; further 2-step prediction, 8.93, 12.08

In summary, the average relative error is low, indicating that the model is reliable (Kong et al. 2022). The predictions (8.93, 12.08 for the next two observations) can be compared with the next time point observations to verify the integrity of the overall process (Chen et al. 2022; Chen et al. 2021; Javed and Cudjoe 2022). Timely warning of any failure points throughout the observation process facilitates systematic adjustment of the development program (Wu et al. 2022).

Results and discussion

The numerical simulation can make up for the deficiencies of insufficient measurement volume of the plate sand filling experiment, and also obtain the following information.

1. The premise of the influence of viscosity, with the increase of crude oil viscosity, the recovery rate is multiplied power decreasing trend. The fitted relationship is as follows: $y = 65.451x^{-0.0695}$.
2. The premise of the influence of the rate of fluid extraction, with the increase in the rate of fluid extraction, the recovery rate gradually increased, a logarithmic upward trend. The fitted relationship equation is: $y = 3.0698\ln(x) + 43.503$.
3. The permeability of the premise, with the increase in the model permeability, the recovery rate gradually increased, in a multiplied power upward trend. The fitted relationship is as follows: $y = 18.898x^{0.1173}$.

The following engineering guidelines can be derived: (1) The highest recovery rate is obtained with 2000 mD permeability, 90 mPa s viscosity, and 5 mL/min fluid extraction rate under the premise of different categories of influencing factors. Therefore, the crude oil viscosity is adjusted to 90 mPa s by means of water blending and dosing, and the 5 mL/min water injection rate is adopted for extraction. (2) The oil recovery wells near the relative water injection wells have high fluid production, but low oil production. This may be due to the disorder of reservoir injection and extraction coupling in the longitudinal direction, so the multi-layer reservoir should be roughly divided into independent injection and extraction units in the upper and lower phases by means of ground switches and downhole separators. According to the physical properties of the sand body reservoir, the layer with good physical properties should be allowed to inject water first and the layer with poor physical properties should be recovered, and the injection and recovery coupling mechanism should be applied to adjust the parameters of injection rate, timing, period, and oil recovery pressure difference between the upper and lower layers for extraction. (3) Under the condition of 2000 mD permeability, 180 mPa s viscosity, and 2 mL/min fluid recovery rate, the average oil production and recovery rate are equal, which may be caused by the randomness of reservoir injection and recovery coupling in the lateral direction. Therefore, the auxiliary alternative of alternating immobile pipe column should be adopted. During the production process, the formation fluid enters the switch body from the liquid hole, flows into the casing through the single flow valve, and is lifted to the surface by the pump. (4) During the mining process, the fitted equations obtained from numerical simulation can be applied to evaluate the reasonableness of the parameters in this stage, identify the issues of this stage, and predict the production trend changes in the next mining period by comparing the production data. The development plan can be adjusted in real time.

Based on the analysis of the experimental results described above and in conjunction with the current development situation in the study area, several development adjustment options can be proposed. Firstly, due to the poor water drive, the fluid production rate has been adjusted to 0.5 mL/min. This may lead to a decrease in the water injection ripple area but increase the advance velocity ratio. Secondly, due to the high viscosity of the crude oil in the study area, water flush measures should be implemented, particularly by adding 2% paraffin scavengers and viscosity reducer based on the size of single well production, with a dosing interval of 2 days and a weekly dosage of 2%. Thirdly, based on the current situation of water flooding and contradictory injection and production in the study area, measures should be taken to block the high permeability layer and combine the medium and low permeability layers to alleviate the uneven injection and production due to the heterogeneity of the reservoir. Fourthly, based on the tongue-in situation in the study area, measures should be taken to adopt pulse-type large-displacement flushing (3 m^3/h) injection for 0–3 h and 6 h shutdown response followed by measures to control oil recovery rate. Fifthly, based on the reservoir characteristics of the Tankou X well area, a chloride ion monitoring and testing system should be used to project the degree of water flooding tongue-in and dynamically adjust injection parameters. Additionally, the use of deep pumping supporting process technology should be implemented to meet well production needs with injection and production being used as the main means of water injection adjustment to increase remaining oil saturation and ultimately achieve the purpose of improving recovery.

Although our research is more targeted, it has lower experimental costs and a shorter research process. Compared to previous studies that conducted large-scale determination of development influencing factors such as injection method, injection timing, injection period, injection rate, and injection viscosity, we have placed more emphasis on combining theory with engineering practice and have used numerical simulations to compensate for the shortcomings in real experiments and extend the degree of application of the results (Ning et al. 2022). The next revision of the development plan cannot be based solely on the recovery rate but needs to consider the influence of both crude oil properties and stable production period (Yongbin et al. 2020). We have constructed the idea of adjusting the development work of old oil areas by subordinating engineering to geology and geology to engineering. However, we still have shortcomings in the coverage of experimental configurations and the generality of development schemes, for example, (1) We only measured experimental data for thick oil samples and did not conduct experimental discussions on conventional crude oil and low-viscosity crude oil; (2) The factors affecting the effect of different well network types and well spacing on the effect of water-driven oil are more complex and have significant implications for field development optimization. Multi-factor interaction experimental design is required, followed by optimization of resources and eventual commencement of experiments. However, due to limited experimental conditions, we did not discuss this; (3) The matching study of different water content and fluid recovery rate is also lacking due to limited experimental conditions and the experimental scheme cannot effectively simulate real working conditions.

Conclusion

(1) Oil production wells close to water injection wells have high liquid production, but low oil production. This may be caused by the disorder of injection-production coupling in the reservoir vertically.
(2) The average fluid production, average oil production, and oil recovery are equal under the premise of 2000 mD permeability, 180 mPa s viscosity, and 2 mL/min fluid production rate, which may be caused by the disorder of injection-production coupling in the reservoir horizontally.
(3) The optimal stable production time is 3000 min, and the maximum oil recovery rate is 47.92% under the premise of 5 mL/min fluid recovery rate. Geologically, when the preconditions are the same, the recovery ratio of 1000 mD is 1.76% lower than that of 2000 mD.
(4) In the next step, it is necessary to broaden the experimental boundary of crude oil viscosity and discuss the influence of different well pattern types and well spacing on water flooding effect.

Funding The project "Study on development technical countermeasures of complex fault block reservoir in Jianghan Oilfield" (JKK0221003) supported the study.

Data availability All data generated or analyzed during this study are included in this published article.

Declarations

Conflict of interest The authors declare that they have no competing interests.

References

Abd-elfattah SS, Abu-Elmaaty AI, Hashim IH (2022) Reliability analysis of flexible pavement using crude Monte Carlo simulation. ERJ J Eng Res 45(3):447–456

Aleidan A, Kwak H, Muller H, Zhou X (2016) Residual oil zone: paleo oil characterization and fundamental analysis. SPE Improved Oil Recovery Conference 143:125

Chen ZY, Meng Y, Chen T (2022) NN model-based evolved control by DGM model for practical nonlinear systems. Expert Syst Appl 193:115873

Chen Xianlei et al (2023) Energy consumption reduction and sustainable development for oil & gas transport and storage engineering. Energies 16(4):1775

Chen, Z. Y., Huang, L., Wu, H., Meng, Y. ang, S., & Chen, T. (2021). Grey signal predictor and evolved control for practical nonlinear mechanical systems. J Grey Syst 33(1)

Escobar LA, Meeker WQ. (2006). A review of accelerated test models. Stat Sci 552-577. https://doi.org/10.1214/088342306000000321

Galetto F (2022) Minitab T charts and quality decisions. J Stat Manage Syst 25(2):315–345

Gao Shusheng et al (2020) A new method for well pattern density optimization and recovery efficiency evaluation of tight sandstone gas reservoirs. Na Gas Ind B 7(2):133–140

Gupta N, Parakh S, Gang T, Cestari N, Bandyopadhyay P (2022) Residual oil zone recovery evaluation and forecast methodology: a Wasson field case study. In: SPE improved oil recovery conference. SPE, p. D031S036R002

Javed SA, Cudjoe D (2022) A novel grey forecasting of greenhouse gas emissions from four industries of China and India. Sustain Prod Consum 29:777–790

Kalpande SD, Toke LK (2022) Reliability analysis and hypothesis testing of critical success factors of total productive maintenance. Int J Qual Reliab Manag 40(1):238–266

Kesarwani H, Srivastava V, Mandal A, Sharma S, Choubey AK (2022) Application of α-MnO 2 nanoparticles for residual oil mobilization through surfactant polymer flooding. Environ Sci Pollut Res 29(29):44255–44270

Kong XH, Deng C, Tang ZQ (2022) Grey DGM (1, 1, f (k, m)) Model and its application in the prediction of per capita natural gas consumption. Int J Uncertainty Innov Res 4(2):117-126

Liao C, Wang R, Zhang J, Huang Q, Li X, Zheng X, Lin Z (2023) Well testing analysis methodology and application for complex fault-block reservoirs in the exploration stage. In: SPE gas & oil technology showcase and conference. SPE, p. D021S028R006

Liu L, Ao Y, Wu Z, Wang X (2022) Hydro-mechanical coupling numerical simulation method of multi-scale pores and fractures in tight reservoir. IOP Conf Ser Earth Environ Sci 983(1):012060

Ma X (2021) Potential reservoir candidates for the construction of UGS facilities in Central and Western China. Handbook of Underground Gas Storages and Technology in China. Singapore: Springer Singapore, pp 511-527

Nan JH (2021) Study and application of resource potential evaluation in complex fault block reservoirs of Hailaer basin. International Field Exploration and Development Conference, pp 2520–2529

Ning X, Wang Z, Wang C, Wu B (2022) Adaptive feedforward and feedback compensation method for real-time hybrid simulation based on a discrete physical testing system model. J Earthq Eng 26(8):3841–3863

Shitana ES, Sony M (2022) Reliability analysis of Keith centrifuge at a meat processing plant in Windhoek, Namibia. Int J Oper Res Inf Syst (IJORIS) 13(1):1–20

Sun L, Cui C, Wu Z, Yang Y, Zhang C, Wang J, Guevara J (2023) A mathematical model of CO_2 miscible front migration in tight reservoirs with injection-production coupling technology. Geoenergy Sci Eng 221:211376

Techarungruengsakul R, Kangrang A (2022) Application of Harris Hawks optimization with reservoir simulation model considering hedging rule for network reservoir system. Sustainability 14(9):4913

Wali ST, Baqer HA (2020) A practical method to calculate and model the petrophysical properties of reservoir rock using petrel software: a case Study from Iraq. Iraqi J Sci 2640-2650. https://doi.org/10.24996/ijs.2020.61.10.20

Wang Yi et al (2017) Experimental investigation of optimization of well spacing for gas recovery from methane hydrate reservoir in sandy sediment by heat stimulation. Appl Energy 207:562–572

Wang ZX, Li DD, Zheng HH (2020) Model comparison of GM (1, 1) and DGM (1, 1) based on Monte-Carlo simulation. Physica A Stat Mech Appl 542:123341

Wang J, Luo J, Fan Y (2023a) Digital fabrication and reliability evaluation method for G-band TWT electron optical system. IEEE Trans Electron Devices 70(5):2548–2555

Wang Q, Bi Y, Zhang Y, Cao T, Liu D (2023b) Study on the influence of different key parameters on EOR in LB block. E3S Web of Conferences 375: 01053

Wu W, Ma X, Zhang H, Tian X, Zhang G, Zhang P (2022) A conformable fractional discrete grey model CFDGM (1, 1) and its application. Int J Grey Syst 2(1):5–15

Ye J, Dang Y, Ding S, Yang Y (2019) A novel energy consumption forecasting model combining an optimized DGM (1, 1) model with interval grey numbers. J Clean Prod 229:256–267

Wu Y, Liu X, Du X, Zhou X, Wang L, Li J, Li Y, Li X, Li Y (2020) Scaled physical experiments on drainage mechanisms of solvent-expanded SAGD in super-heavy oil reservoirs. Petroleum Exploration and Dev 47(4): 820-826

Yunsheng L, Lou J, Minghua L, Libin G, Juanmei Y (2017) Structural model and exploration potential in Tankou block of Qianjiang sag, Jianghan Basin. China Petroleum Exploration 22(4):84

Zhai H, Jin G, Liu L, Su Z, Zeng Y, Liu J, Li G, Feng C, Wu N (2023) Parametric study of the geothermal exploitation performance from a HDR reservoir through multilateral horizontal wells: the Qiabuqia geothermal area, Gonghe Basin. Energy 275:127370

Zhao H, Han X, Guo S (2018) DGM (1, 1) model optimized by MVO (multi-verse optimizer) for annual peak load forecasting. Neural Comput Appl 30:1811–1825

Zheng S, Sharma M (2022) Coupling a geomechanical reservoir and fracturing simulator with a wellbore model for horizontal injection wells. Int J Multiscale Comput Eng 20(3). https://doi.org/10.1615/intjmultcompeng.2021039958